RSC Advances


This is an *Accepted Manuscript*, which has been through the Royal Society of Chemistry peer review process and has been accepted for publication.

*Accepted Manuscripts* are published online shortly after acceptance, before technical editing, formatting and proof reading. Using this free service, authors can make their results available to the community, in citable form, before we publish the edited article. This *Accepted Manuscript* will be replaced by the edited, formatted and paginated article as soon as this is available.

You can find more information about *Accepted Manuscripts* in the Information for Authors.

Please note that technical editing may introduce minor changes to the text and/or graphics, which may alter content. The journal's standard Terms & Conditions and the Ethical guidelines still apply. In no event shall the Royal Society of Chemistry be held responsible for any errors or omissions in this *Accepted Manuscript* or any consequences arising from the use of any information it contains.

ROYAL SOCIETY OF CHEMISTRY

www.rsc.org/advances

Please do not adjust margins

RSC Advances

Paper

# Chemical synthesis of 3D copper sulfide with different morphologies for high performance supercapacitors application

Received 00th January 20xx,
Accepted 00th January 20xx

DOI: 10.1039/x0xx00000x

www.rsc.org/

Ravindra N. Bulakhe[a], Sumanta Sahoo[a], Thi Toan Nguyen[a], Chandrakant D. Lokhande[b], Changhyun Roh[c], Yong Rok Lee,[a] Jae-Jin Shim[a]*

**Abstract:** 3D copper sulfide ($Cu_2S$) with different morphologies for high performance supercapacitors were synthesized via a simple, costeffective successive ionic layer adsorption and reaction (SILAR) method. Further these $Cu_2S$ nanostructure demostrate excellent surface properties like uniform surface morphology, large surface area of $Cu_2S$ samples. X-ray diffraction (XRD) X-ray photoelectron spectroscopy (XPS) and Raman spectroscopy of these samples confirmed the crystallinity and crystal structure of $Cu_2S$. The electrochemical studies of $Cu_2S$ samples have been investigated by cyclic voltammetry, charge-discharge and electrochemical impedance spectroscopy techniques. The maximum specific capacitance of flower like and integrated nanotubes samples are found 761 and 470 F $g^{-1}$ respectively, at a scan rate of 5 mV $s^{-1}$. The electrodes are prepared using a simple four-beaker SILAR system at ambient conditions, thus providing an easy approach to fabricate high-power and high-energy supercapacitors. Further, the EIS analysis shows lower ESR value, high power performance, excellent rate as well as frequency response to flower like $Cu_2S$ sample. The Ragone plot shows better power and energy densities of all $Cu_2S$ nanostructured samples. The long-term cycling performance of $Cu_2S$ is examined with excellent retenation of 95%. The high surface area provided by the porous and more conductive 3D nickel foam have been utilized properly to enhance the electrochemical properties of copper sulfides with charge transport and storage.

## 1. Introduction

Nowadays, there has been needs to develop energy storage and conversion devices from alternative energy sources due to limited reserve of fossil fuels.[1,2] The electrochemical energy storage and conversion devices include batteries, fuel cells, electrochemical capacitors (ECs), etc.[3] Among them, supercapacitors have several advantages such as high power density, a fast charge-discharge process, long-term stability and low maintenance cost.[4] Generally, in supercapacitor energy can store either ion adsorption (EDLCs, electrical double-layer capacitors supercapacitors) or surface redox reactions (pseudocapacitors).[5] Generally, pseudocapacitors have much higher power and energy densities than electrical double-layer capacitors because of their fast and reversible redox reactions (several tens of nanometers from the surface). Therefore, pseudocapacitors have been attracted widely. [6–11]

Generally, the materials used for electrochemical energy storage devices are metal oxides, polymers, composites, metal sulfides and carbon materials, such as carbon nanotubes and graphene.[12-16] Of these, carbon materials are expensive and the polymer materials are environmentally unstable and tend to degrade. Metal oxides, however, are moderate in cost but they are not stable for long cycle life. Metal sulfides are cheap with moderate stability, similar to metal oxides. Metal sulfides has advantageous in the case of supercapacitive studies because of their unique physical and chemical properties (e.g., higher electrical conductivity, mechanical and thermal stability than those of their corresponding metal oxides), as well as the rich redox chemistry that contributes to their high specific capacitance (several times higher than those of carbon/graphite-based materials), environmental friendliness, low toxicity, and abundance in nature; therefore, it is considered a promising lucrative pseudocapacitive material in supercapacitors.[17]

Very few researchers have used this material in energy storage devices. Metal sulfides, such as lead sulfides, zinc sulfides, cadmium sulfides, copper sulfides, bismuth sulfides, and nickel sulfides, are inorganic materials that have attracted the attention of researchers for their unique properties and potential applications.[18-23] Among these materials, copper sulfide ($Cu_xS$ with x = 1-2) is a transition metal chalcogenide that exhibits different stoichiometric forms according to the

[a] School of Chemical Engineering, Yeungnam University, Gyeongsan, Gyeongbuk, 712-749, Republic of Korea.
[b] Thin Film Physics Laboratory, Department of Physics, Shivaji University, Kolhapur-416 004, (M.S.), India.
[c] Radiation Research Division for Biotechnology, Advanced Radiation Technology Institute, Korea Atomic Energy Research Institute, 989-111 Daedeok-daero, Yuseong-gu, Deajeon 305-353, Republic of Korea.

†Electronic Supplementary Information (ESI) available: The schematic representations of the SILAR method (S1), the SAED pattern of materials (S2) and electrochemical formulae (S3). See DOI: 10.1039/x0xx00000x

RSC Advances Accepted Manuscript



Please do not adjust margins

crystal structure ranging from orthogonal to hexagonal. The shape, size, stoichiometric composition, and crystal structure generally control the optical and electrical properties of copper sulfide.[24] Copper sulfide with five different stoichiometries, such as covellite (CuS), anilite ($Cu_{1.75}S$), digenite ($Cu_{1.8}S$), djurlite ($Cu_{1.95}S$), and chalcocite ($Cu_2S$) are stable at room temperature.[25] A maximum specific capacitance of 487.8 F $g^{-1}$ in 1 M KCl electrolyte is reported by Shi et al. for $Cu_2S$ prepared using electron beam evaporation and sulfurization method.[26] Also Stevic et al. reported maximal specific capacitance of 200 F $cm^{-1}$ for electrochemically deposited $Cu_2S$ on copper wire.[27]

Many researchers have been attempted to improve the properties of materials using different physical and chemical methods. In physical method, sophisticated and expensive instruments are required for their preparation. Large area deposition is very difficult using physical method. Therefore, chemical methods have been widely used to overcome on these difficulties. Chemical methods include chemical bath deposition (CBD) method, electrodeposition method, chemical vapour deposition (CVD) method and the successive ionic layer adsorption and reaction (SILAR) method. Among them, the SILAR method can be used to prepare large area electrodes in less time in a cost-effective manner.[28, 29]

In the present study, first time we report a fabrication of 3D porous copper sulfide electrode via a very simple, cost effective SILAR method at ambient temperature and its improved supercapacitive properties. Two different complexing agents play a vital role in the different morphologies of copper sulfides, directly grown on conductive substrates. The supercapacitive performance of these nanomaterials is investigated in the terms of specific capacitance, energy and power densities and good electrochemical stability. The obtained results will be helpful for constructing $Cu_2S$ electrodes for solid state energy storage devices.

## 2. Experimental Section

### Materials synthesis

The three dimensional (3D) nickel foam (NF) electrodes were cleaned by dilute HCl predeposition of materials. The simple and cost effective SILAR method was investigated to synthesis of copper sulfide using copper sulfate as a copper source. The liquid ammonia solution (AMM) and hexamethyltetrammine (HMT) were used as the complexing agents. Thiourea was used for sulfur source. For rinsing purposes, deionized water (D. I.) was used in between the two precursors. Briefly, a 0.1 M copper sulfate solution was prepared in 100 ml D. I. water using two different complexing agents (AMM and HMT) separately. After adding an excess ammonia solution, the pH of the solution was maintained at ~ 10 then used as the copper precursor. For the sulfur precursor, thiourea was used separately for an AMM/HMT complexing agent bath. The same procedure was employed separately for both baths (each complexing agent) for deposition at ambient temperature using unstirred solutions. In the SILAR method, the concentration, pH, temperature of the precursor solutions, durations of adsorption, reaction, and rinsing are important. By performing several experiments, the $Cu_2S$ electrodes deposition condition was optimized and deposition was carried out. Finally, the prepared samples were called Cu:AMM for liquid ammonia solution and Cu:HMT for the hexamethyltetrammine complexing agents, respectively.

### Material characterization

The prepared electrodes (Cu:AMM and Cu:HMT) were characterized structurally by X-ray diffraction (XRD), X-ray photoelectrons spectroscopy (XPS), Raman spectroscopy and characterized morphologically by field emission scanning electron microscopy (FE-SEM), and transmission electron microscopy (TEM). XRD (PANalytical) was carried out using target Cu $K_{\alpha}$ radiation. The morphology of the compounds was examined by FE-SEM (HITACHI, LTD S-4800). TEM was carried out by STEM spectroscopy (model CM 200). The XPS was carried out using a model K-Alpha spectrometer. Raman spectroscopy was carried out using a model XploRA plus (HORIBA) Raman spectrometer. Electrochemical characterization was performed using an AutoLab Potentiostat in a 1 M KOH solution. The electrochemical measurements were carried out using a three electrode configuration cell in 1 M KOH as the electrolyte. $Cu_2S$ nanostructured electrodes (Cu:AMM/Cu:HMT) on 3D nickel foam were used directly as the working electrode, platinum electrode as the counter and SCE as the reference electrodes. The electrochemical performance of the prepared electrodes was characterized by cyclic voltammetry, galvanostatic charge-discharge cycling stability and electrochemical impedance spectroscopy using Auto Lab with Nova 1.10 software, Netherland.

## 3. Results and Discussion

### 3.1. Film Formation and Reaction Mechanism

FILM FORMATION

Schematic representation of the SILAR method shown in the supporting information S1 for the deposition of copper sulfides (Cu:AMM/Cu:HMT). Briefly, a four-beaker system was used, in which beaker 'A' consists of an aqueous solution of 0.1M copper sulfate ($CuSO_4$) as the cationic precursor and 0.1 M AMM/HMT as the complexing agent. The reaction with thiourea ($H_2NCSH_2N$) was carried out in beaker 'C' using 0.01 M thiourea solution (pH~ 6) as an anionic precursor as well as a reducing agent to reduce $Cu^{2+}$ to $Cu^{+}$. Beakers, 'B' and 'D', with D. I. water were used for rinsing. The NF was immersed in beaker 'A' consisting a cationic precursor for 20 s. Copper ions were adsorbed on the surface of the substrate and the un-adsorbed ions were removed by rinsing the NF in beaker 'B' consisting of D. I. water for 30 s. For the reaction with $S^{2-}$ ions, the NF was immersed in beaker 'C' containing an anionic precursor (thiourea) for 20 s. The powdery material or loosely bounded ions were removed by rinsing the substrate in beaker 'D' containing D. I. water for 30 s. This completes a single SILAR cycle. Such SILAR cycles were repeated 100 times to

RSC Advances Accepted Manuscript


This journal is © The Royal Society of Chemistry 20xx

obtain the optimal thickness. According to the growth kinetics, the film grows by ion-by-ion deposition at the nucleation sites on the immersed surface.

**REACTION MECHANISM**

0.1 M $CuSO_4$, as the copper source, as added to an aqueous ammonia ($NH_4OH$) solution with constant stirring to make the solution alkaline. Initially, when the aqueous ammonia solution was added to copper sulfate, the ion product of $Cu(OH)_2$ exceeded the solubility product, and the solution became turbid due to the precipitation of Cu $(OH)_2$, such as

$$CuSO_4 + 2NH_4OH \rightarrow Cu(OH)_2 + 2NH_4^+\downarrow + SO_4^{2-} \quad \text{.....(1)}$$

Moreover, the addition of an excess ammonia solution reduced the concentration of $Cu^{2+}$ ions by producing the complex ion, $Cu(NH3)_n^{2+}$ (n = 1 to 4), with n = 4 being the most stable co-ordination number.[30] Owing to complex formation, the solution became clear and transparent, which may obey the following reaction:

$$Cu(OH)_2 + 4NH_4^+ \rightarrow Cu(NH_3)_4^{2+} + 2H_2O + 2H^+ \quad \text{.....(2)}$$

When the substrate was immersed in the first beaker solution, the $Cu(NH3)_n^{2+}$ ions in the solution were adsorbed on the NF because of the force of attraction between the $Cu(NH3)_n^{2+}$ ions and the NF. These forces may be cohesive, van der Waals, or other chemical attractive or electrostatic forces. A similar type of reaction occurs with HMT as follows:

$$(CH_2)_6N_4 + 6H_2O \rightarrow 6HCHO + 4NH_3 \quad \text{..... (3)}$$

This follows reactions (2) and (3) similarly.

The aqueous thiourea solution provides a source of $S^{2-}$ ions and thiourea acts as reducing agents ($Cu^{2+}$ to $Cu^+$), which provides an alternative path for the reaction by reducing the activation energy of the chemical reaction as follows:

Dissociation of thiourea in an alkaline medium

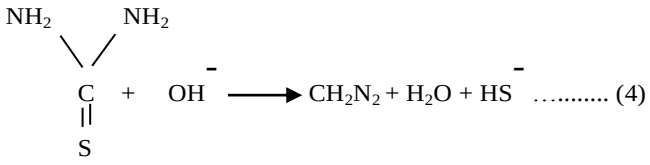


..... (4)

Formation of divalent sulfide ions

$$HS_2 + OH^- \longrightarrow S^{2-} + H_2O \quad \text{..... (5)}$$

The reaction was followed by the immersion of wet NF into a thiourea solution maintained at 300 K, where the chemical reaction between $S^{2-}$ and the preadsorbed $Cu(NH3)_n^{2+}$ ions at the surface of the NF results in the deposition of an adherent $Cu_2S$ layer a few nanometers in thickness according to reaction (6),

$$Cu(NH_3)_4^{2+} + S^{2-} \rightarrow Cu_2S + 4NH_3\uparrow \quad \text{..... (6)}$$

The cycle of ion adsorption followed by an oxidation reaction was repeated several times to achieve different film thicknesses. This step completed a single SILAR cycle. The cycle was repeated 100 times. Finally, the NF decorated $Cu_2S$ was rinsed several times with deionized water to remove the loosely bound and unreacted species.[25, 29-30]

### 3.2. Structural Studies (XRD, XPS and Raman)

The film crystallinity was examined by XRD. Fig.1 shows the XRD pattern of copper sulfide decorated nickel foam (NF). The peaks at 44.3, 51.8 and 76.2° 2θ corresponds to NF (Fig.1 (a)). Figs. 1 (b) and Fig. 1 (c) shows the XRD patterns of the Cu:AMM and Cu:HMT electrodes, respectively. The (2 1 0) plane was more intense compared to the other planes. The (2 1 0) and (1 0 1) planes were in good agreement with the JCPDS card no. 026-1116 for a hexagonal phase. The (1 1 0) plane belongs to digenite and (1 2 12) plane belongs to orthorhombic phase (JCPDS card no. 002-1281 and 002-1272). Therefore, the formation of polycrystalline and mixed phase of copper sulfide was confirmed.[25, 31] Owing to the mixed phase formation of copper sulfide; it may enhance the stability and electrochemical performance.

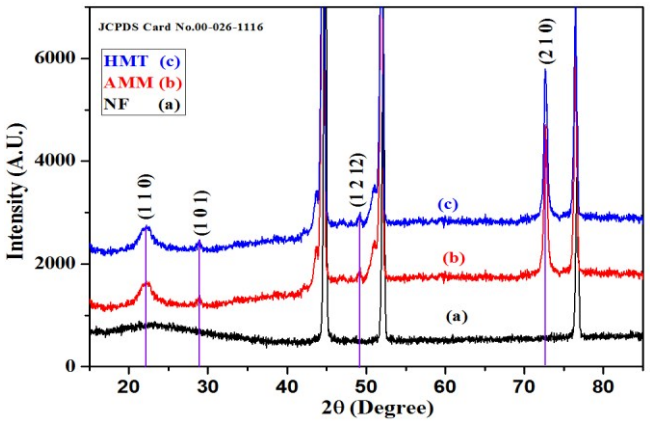


**Fig.1:** XRD patterns of (a) Nickel foam, (b) Cu:AMM and (c) Cu:HMT electrodes.

XPS study was carried out to obtain the detailed information on the chemical state of Cu:AMM and Cu:HMT samples, as shown in Fig.2. The full survey (Fig.2a) indicates the presence of Cu and S and no other impurities could be found on the surface of the $Cu_2S$ electrodes. The XPS was corrected with O 1s baseline, which was assigned a binding energy of 532.4 eV (Fig.2b). Fig. 2c presents the XPS spectra of the Cu2p core level. The peaks at a binding energy (B.E) of 932.3 and 952.1 eV were assigned to $Cu2p_{1/2}$ and $Cu2p_{3/2}$, indicating the presence of $Cu^{2+}$ on the surface of the electrodes. The peaks assigned to 963.4 and 944 eV (2d) correspond to satellite peaks. The spin orbit splitting is the difference between the binding energy of Cu $2p_{3/2}$ and Cu $2p_{1/2}$ levels was observed at 19.8 eV. The S 2p spectrum was fitted to the spin orbit doublet assigned to binding energies of 163.5 and 168.4 eV for $2p_{3/2}$ and Cu $2p_{1/2}$ peaks, respectively. Therefore, the above results confirm the formation of $Cu_2S$, which matches the XRD data. [32-34]

RSC Advances Accepted Manuscript

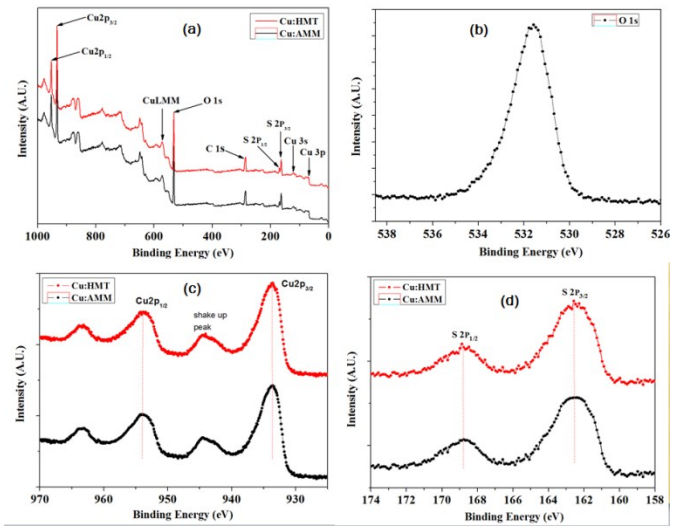


**Fig.2:** (a) Full XPS spectra of $Cu_2S$ nanostructures synthesized from different complexing agents, (b) core-level XPS of O1s, (c) core-level XPS spectra of Cu2p for Cu:AMM, and Cu:HMT samples and (d) core-level XPS of S2p for Cu:AMM, and Cu:HMT sample.

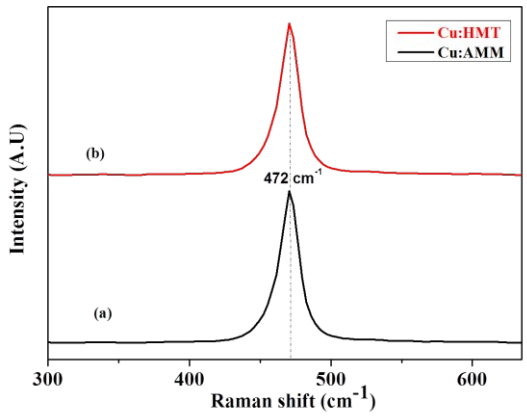


**Fig. 3:** Raman spectra of $Cu_2S$ for Cu:AMM, and Cu:HMT samples.

Raman spectroscopy is an effective tool for examining the material structure, so it is suitable for exploring the surface layer structure of nanometer-sized crystals of $Cu_2S$. Until now, there have been very few reports on the Raman characterization of nanostructured $Cu_2S$ films. Fig. 3 (a, b) shows the Raman spectra of the typical nanostructured $Cu_2S$ samples (Cu:AMM and Cu:HMT). This study revealed the Raman shifts of $Cu_2S$ for the Cu:AMM and Cu:HMT samples, i.e., a strong and sharp band at 472 $cm^{-1}$. Similar results were reported by Su et.al.[35] In addition, Tang et al. also reported similar results of $Cu_2S$.[36]

### 3.3. Surface Morphology studies

To understand the morphology, FE-SEM was performed of Cu:AMM and Cu:HMT electrodes and results are shown in Fig. 4. The wide porous NF skeleton is decorated with copper sulfide, as shown in the low magnification SEM images (Fig. 4a, e). Fig. 4b, f shows the well overgrown copper sulfide materials completely covering the NF. The overgrowth occurred due to increases in the number of adsorbed ions by the several numbers of repeated cycles. Fig. 4c shows flower-like structures grown on the NF with a mean size of 500 nm. At higher magnifications, the integrated nanoflakes of 15 nm in width (Fig. 4d) and integrated nanowire of 50 nm in length (Fig. 4h) were observed on the Cu:AMM and Cu:HMT electrodes, respectively. These integrated nanoflakes/nanowires were interconnected with each other to form flower like structures.

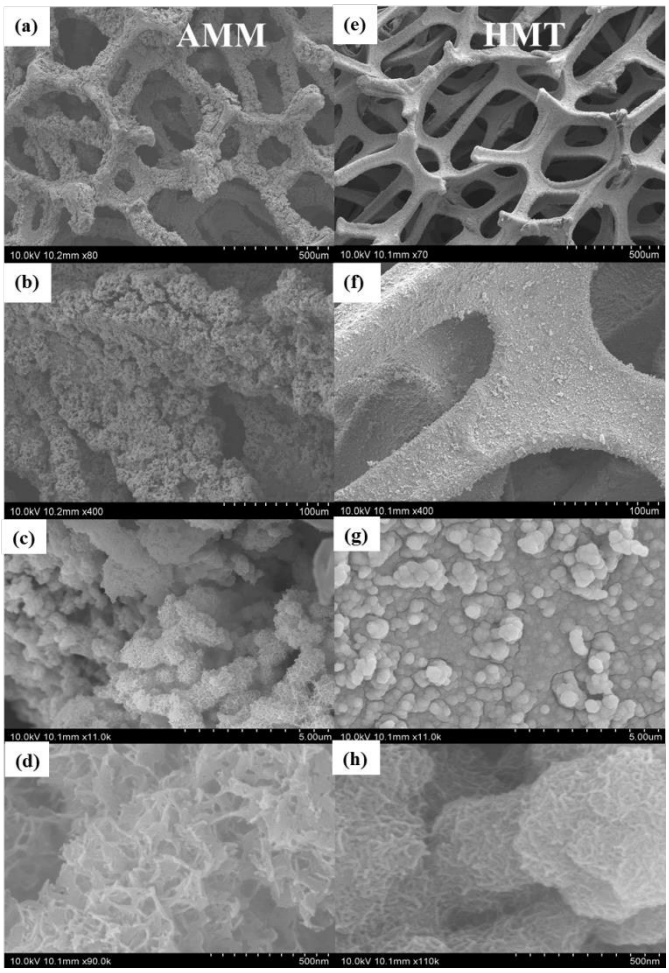


**Fig.4:** SEM images of Cu:AMM (a-d) and Cu:HMT (e-h) on the nickel foam at different magnifications.

A detailed schematic of the probable steps involved in the formation of $Cu_2S$ is shown in fig.5. i) Initially $Cu^+$ ions are adsorbed on the surface of substrate then $S^{--}$ ions attached to ions $Cu^+$ from cationic and anionic precursor ii) $Cu^+$ and $S^{--}$ ions combines on the substrate to form layer by layer $Cu_2S$ nuclei. iii) Continued growth of $Cu_2S$ crystals, form a flower like/ nano wire structures for Cu:AMM and Cu:HMT electrodes, respectively. iv) The actual SEM image is shown for Cu:AMM and Cu:HMT electrodes. Liu and Sun reported similar types of morphologies.[37] Kaner et al. also reported an incorporated flower-like structure for polyaniline electrodes by the chemical oxidation method.[38]

RSC Advances Accepted Manuscript



This journal is © The Royal Society of Chemistry 20xx

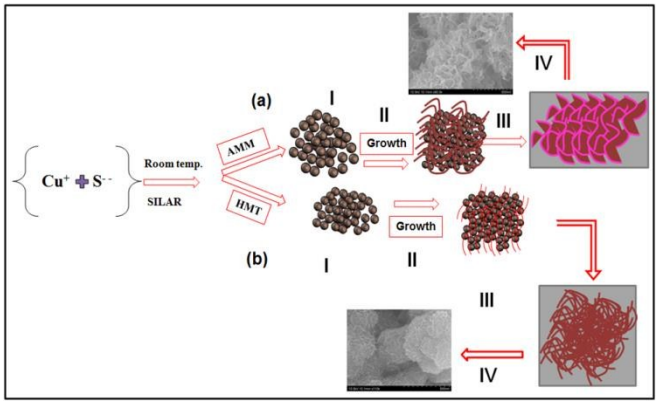


**Fig. 5:** (a, b) shows schematic of probable steps involved in the formation of $Cu_2S$.

Fig. 6 presents HR-TEM images of copper sulfide electrodes. Fig. 6(a, d) shows HR-TEM images of Cu:AMM and Cu:HMT electrodes at higher magnification (20 nm), respectively. The porous part reflects the thicker flake like structure for Cu:AMM and the nanotube like structure belongs to the Cu:HMT electrodes observed in Fig.6(a, d). At higher resolution, the planer structure was observed (Fig. 6(b, e)). A similar clear plane to that in the XRD (101) peak with an inter spacing distance of d=3.012 and 3.105 Å for Cu:AMM and Cu:HMT electrodes (Fig.(6c, f)), respectively, was observed.[39] The SAED pattern of both electrodes are shown in supporting information S2.

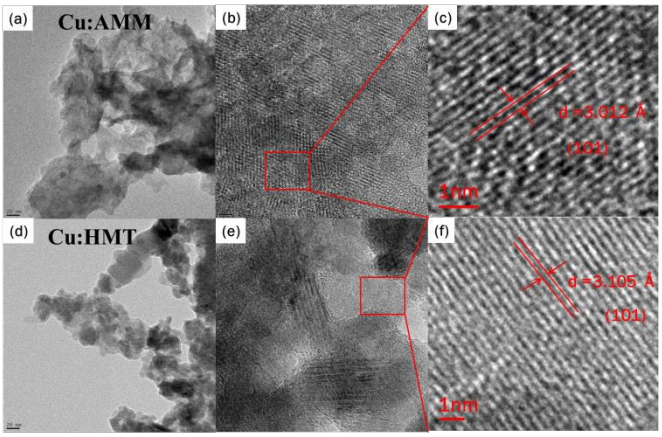


**Fig.6**: TEM images of Cu:AMM (a-c) and Cu:HMT (d-f) electrodes, respectively.

### 3.4. Supercapacitive Performance

The supercapacitive performance of the Cu:AMM and Cu:HMT electrodes was performed using a three electrode system. This contains Cu:AMM/Cu:HMT as the working electrode, platinum as the counter electrode and saturated calomel electrode (SCE) as the reference electrode. Fig. 7a shows the cyclic voltammograms of NF as a reference, Cu:AMM and Cu:HMT electrodes in an aqueous 1 M KOH solution at a scan rate of 5 mV $s^{-1}$. Fig. 7b shows the specific capacitance as a function of the scan rate for the Cu:AMM and Cu:HMT electrodes. The Cu:AMM and Cu:HMT electrodes showed a maximum specific capacitance of 761 and 470 $Fg^{-1}$, respectively, at a scan rate of 5 mV $s^{-1}$. The specific capacitance decreased from 761 to 602 and 470 to 340 $Fg^{-1}$ as the scan rate was increased from the 5 to 100 mV $s^{-1}$ for the Cu:AMM and Cu:HMT electrodes, respectively. The values were calculated using the formula given in the supporting data S3. As the scan rate increased, the specific capacitance decreased, indicating that the electrodes material had supercapacitive behavior. Fig. 7(c, d) shows the effect of the scan rate variation on the CV behaviour of Cu:AMM and Cu:HMT electrodes. The decrease in capacitance was attributed to the presence of inner active sites, which cannot sustain the redox transitions completely at higher scan rates. This is probably due to the diffusion effect of protons within the electrode. The decreasing trend of the capacitance suggests that parts of the electrode surface of the electrode were inaccessible at high charging and discharging rates. Yu et al. reported a maximum specific capacitance of 487.8 F $g^{-1}$ prepared by an electron beam evaporation and sulfurization method.[26] In addition; Stevic et al. reported a maximum specific capacitance of 200 F $cm^{-2}$ by electrochemically deposited $Cu_2S$.[27] The specific capacitance reported in the present study was higher other than the copper sulfide electrodes reported earlier. This may be due to (i) the 3D porous interconnected conducting framework of nickel foam, and (ii) the flower-like porous nanomaterial of the copper sulfide material.[40]

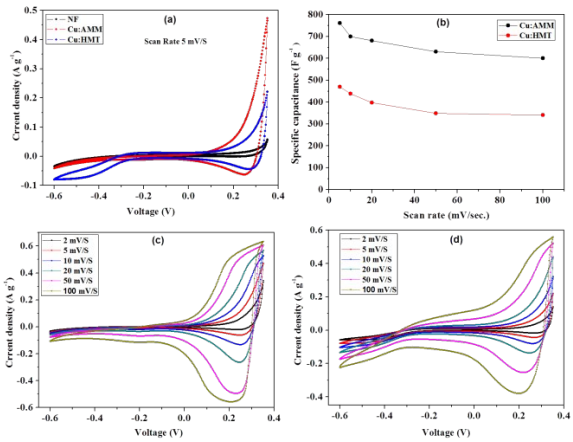


**Fig.7:** Electrochemical studies of Cu:AMM and Cu:HMT electrodes. (a) Cyclic voltammograms within the optimized potential range in aqueous 1M KOH at a scan rate of 5 mV $s^{-1}$. (b) Graph of the various scan rate dependent specific capacitance. (c) and (d) Voltammetric response of Cu:AMM and Cu:HMT electrodes at different scan rate.

Fig. 8(a, b) shows the galvanostatic charge-discharge curves of Cu:AMM and Cu:HMT electrodes measured in the 1 M KOH electrolyte with current densities 6, 8 and 10 A $g^{-1}$. The specific capacitance was calculated using the formula given in S3. The maximum specific capacitance obtained for the Cu:AMM and Cu:HMT electrodes was 765 and 587 F $g^{-1}$, respectively. The specific energy and specific power were determined by formula given in S3. The Ragone plot was plotted using the energy density vs. power density for the Cu:AMM and Cu:HMT electrodes, as shown in Fig. 8c. The energy density, specific power density and coulombic efficiency (η) were calculated using the equations given in supporting information S3.The maximum power densities were 12.2 and 2.7 KW $kg^{-1}$ for

RSC Advances Accepted Manuscript

Cu:HMT and Cu:AMM electrodes, respectively. And energy densities were 25.10 and 19.30 Wh $kg^{-1}$ for Cu:AMM and for Cu:HMT electrodes, respectively. The inset in Fig. 8c shows the plots of specific capacitances versus current densities at 6, 8 and 10 A $g^{-1}$. As current density was increased from 6 to 10 A $g^{-1}$, the specific capacitance decreased. This suggests that the material shows supercapacitive behaviour, as shown in Fig.8 (a, b). In addition, the curves are not an ideal straight line, indicating that the process is a faradic reaction. There is an initial drop in potential caused by the internal resistance. The coulombic efficiency (η) was calculated to be 70 and 83 % for Cu:AMM and Cu:HMT electrodes, respectively. [39, 41]

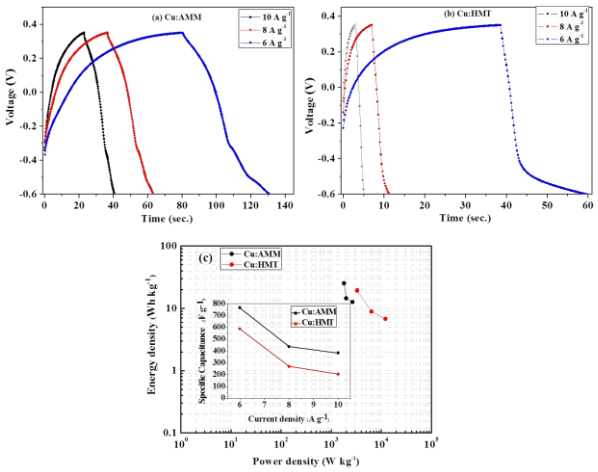


**Fig.8:** Galvanostatic charge–discharge cycling of (a) Cu:AMM and (b) Cu:HMT electrodes in 1 M KOH solution. (c) Ragone plot for Cu:AMM and Cu:HMT electrodes at different current densities. The inset fig. shows a graph of the specific capacitance with different current densities.

Stability is one of the most important parameters in an electrochemical study. The stability of the electrode needs to check before using long term applications. Fig. 9(a, b) shows the cyclic stability of the Cu:AMM and Cu:HMT electrodes at a scan rate of 100 mV $s^{-1}$ for the 1st to 2000th cycle. Fig. 9c shows the variation of the cycle number with the specific capacitance of the Cu:AMM and Cu:HMT electrodes, respectively. The Cu:AMM and Cu:HMT electrodes exhibited 95 % and 93 % cyclic stability over the 2000 cycles. The specific capacitances for Cu:AMM and Cu:HMT electrodes decreased from 602 to 572 F.$g^{-1}$ and 340 to 317 from the 1st to 2000th cycles, respectively. The decrease in specific capacitance may be due to the loss of active material caused by the dissolution and/or detachment, during the early charging/discharging cycles in the electrolyte.[39] Fan et al. reported that the cyclic stability of copper sulfide electrodes synthesized by a one-step solvothermal method was 75.24 % over 500 cycles.[42] In the present case, Cu:AMM has better stability than Cu:HMT.[43]

Fig. 9d shows the Nyquist plots of the Cu:AMM and Cu:HMT samples Performed in 1 M KOH electrolyte, over the frequency range from 10 MHz to 0.01 Hz. An intercept at the high frequency region with the real part (Z) was attributed to the equivalent series resistance (ESR= 1.19, 1.92 Ω), indicating small ohmic loss during discharge.

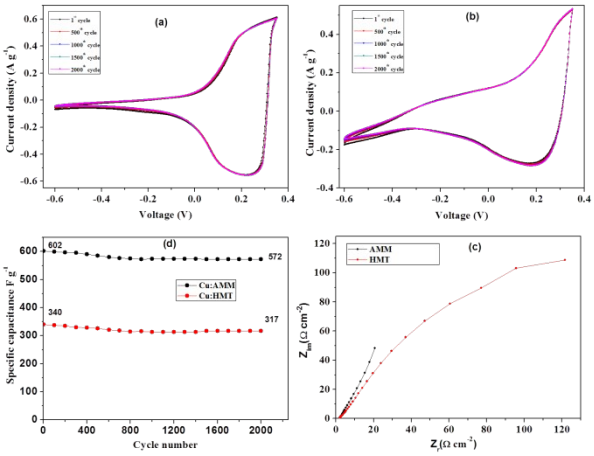


**Fig.9:** Cyclic stability of (a) Cu:AMM and (b) Cu:HMT electrodes at two different cycles in the potential range of +0.35 to – 0.65 V in 1 M KOH electrolyte. (c) Nyquist plots of Cu:AMM and Cu:HMT electrodes over the frequency range, 10 MHz to 0.01 Hz.

In contrast, the distorted semicircle was the charge-transfer process at the electrode electrolyte interface. The distorted semicircle was not observed in the high frequency region, which results in a straight line, indicating the low charge transfer resistance for electrodes. The Warburg resistance was quite small (20 Ω) for Cu: AMM compared to the Cu:HMT (121 Ω) electrodes. The Warburg impedance, W, is associated with the diffusion of the OH- ions produced by the reactions occurring the electrolyte.44 Until now there are very few reports are available on Cu2S supercapacitor so Cu2S is compared with other metal sulfides. The following table.1 describes the comparative data of supercapacitive parameters of metals sulfides.

Table1: comparative data of different supercapacitor parameter of various metal sulfides.

| Materials | Specific Capacitance (F g-1) | Energy Density (Wh $kg^{-1}$) | Power Density (KW $kg^{-1}$) | Ref. |
|---|---|---|---|---|
| $Cu_2S$ | 765 | 25.10 | 12.2 | **Present work** |
| $Cu_2S$ | 587 | 19.30 | 2.7 | **Present work** |
| $Cu_2S$ | 487.8 | - | - | 26 |
| $Cu_2S$ | 200 (F $cm^{-2}$) | - | - | 27 |
| CuS | 305 | 70.8 | - | 39 |
| $CoS_x$ | 475 | - | - | 45 |
| CoS | 138 | 13.2 | 17.5 | 46 |
| SnS | 6.29 | | - | 47 |
| NiS | 618 | - | - | 48 |
| γ-MnS | 240.8 | - | - | 49 |

RSC Advances Accepted Manuscript



This journal is © The Royal Society of Chemistry 20xx

## 4. Conclusions

Nanostructured 3D porous (Cu:AMM and Cu:HMT) electrodes, were successfully synthesized on nickel foam by the simple and cost effective SILAR method and their performance in supercapacitor was studied. As a morphology and electrochemical performance of copper sulfide can be varied by consequence of different complexing agents. The maximum specific capacitance of the Cu:AMM and Cu:HMT electrode was 765 and 587 F $g^{-1}$, respectively. The Cu:AMM and Cu:HMT electrodes showed a specific energy of 25.10 and 19.30 Wh $kg^{-1}$ and a specific power of 12.2 and 2.7 kW $kg^{-1}$, respectively, in a 1 M KOH electrolyte. The Cu:AMM and Cu:HMT electrodes using 3D conducting nickel foam achieved a high specific capacitance. This simple approach may provide a convenient chemical route for the synthesis of Cu:AMM and Cu:HMT as an efficient electrode in high energy storage applications. These finding suggests the copper sulfide is promising electrode material with excellent capacitive behavior and may open up great opportunity in energy storage devices.

## Acknowledgments

This work was supported by the 2015 Yeungnam University Research Grant.

## Notes and references

1 A. S. Arico, P. Bruce, B. Scrosati, J. M. Tarascon and W. V. Schalkwijk, Nat. Mater., 2005, 4, 366-377.
2 Y. Huang, J. Liang and Y. Chen, Small, 2012, 8, 1805-1834.
3 X. Zhao, B. M. Sanchez, P. J. Dobson and P. S. Grant, Nanoscale, 2011, 3, 839-855.
4 Y. Wang, Z. Hong, M. Wei and Y. Xia, Adv. Funct. Mater., 2012, 22, 5185-5193.
5 U. M. Patil, J. S. Sohn, S. B. Kulkarni, S. C. Lee, H. G. Park, K. V. Gurav, J. H. Kim, and S. C. Jun, ACS Appl. Mater. Interfaces 2014, 6, 2450−2458.
6 V. H. Nguyen and J. J. Shim, J. Power Sources, 2015, 273, 110-117.
7 G. A. Snook, P. Kao and A. S. Best, J. Power Sources, 2011, 196,1-12.
8 J. T. Zhang, J. W. Jiang, H. L. Li and X. S. Zhao, Energy Environ. Sci., 2011, 4, 4009-4015.
9 H. Jiang, T. Zhao, C. Z. Li and J. Ma, J. Mater. Chem., 2011, 21, 3818-3823.
10 J. Y. Ji, L. L. Zhang, H. X. Ji, Y. Li, X. Zhao, X. Bai, X. B. Fan, F. B. Zhang and R. S. Ruoff, ACS Nano, 2013, 7, 6237-6243.
11 U. M. Patil, K. V. Gurav, V. J. Fulari, C. D. Lokhande and O. S. Joo, J. Power Sources, 2009, 188, 338-342.
12 A. D. Jagadale, V. S. Kumbhar, R. N. Bulakhe and C. D. Lokhande, Energy, 2014, 64,234-241.
13 B. H. Patil, R. N. Bulakhe and C. D. Lokhande, J. Mater. Sci.: Mater. Electron., 2014, 25, 2188–2198.
14 P. R. Deshmukh, R. N. Bulakhe, S. N. Pusawale, S. D. Sartale and C. D. Lokhande, RSC Advances, 2015, 36, 28687-28695.
15 S. J. Patil, R. N. Bulakhe and C. D. Lokhande, Chempluschem, 2015, 80, 1478-1487.
16 S. Kalathil, V. H. Nguyen, J. J. Shim, M. M. Khan, J. Lee, and M. H. Cho, J. Nano. Nanotech. 2013, 13, 7712−7716.
17 V. H. Nguyen and J. J. Shim, Electrochem. Acta, 2015, 166, 302–309.
18 S.V. Patil, P. R. Deshmukh and C. D. Lokhande, Sens. Actuat. B, 2011, 156,450–455.
19 J. S. Roy, T. Pal Majumder, R. Dabrowski , A. Dey and P. P. Ray, Opt. Mater., 2015, 46,467–471.
20 L. Ma, Y. Chen, Z. Wei, H. Cai, F. Zhang and X. Wu, Appl. Surf. Sci., 2015, 349,740–745.
21 C. Song , H. Yin , N. Zhang , S. Li , B. Zhao and K. Yu, Mater. Lett., 2014, 137,56–58.
22 A. A. Tahir, M. A. Ehsan, M. Mazhar, K. G. U. Wijayantha, M. Zeller and A. D. Hunter, Chem. Mater., 2010, 22, 5084−5092.
23 H. C. Tao, X. L. Yang, L. L. Zhang and S. B. Ni, J. Electro. Chem. 2015, 739, 36–42.
24 Y. Zhao, H. Pan, Y. Lou, X. Qiu, J. Zhu, and C. Burda, J. Am. Chem. Soc. 2009, 131,4253–4261.
25 J. Kundu, and D. Pradhan, Appl. Mater. Interfaces, 2014, 6, 1823−1834.
26 C. Shi, H. Dong, R. Zhu, H. Li, Y. Sun, D. Xu, Q. Zhao, D. Yu, Nano Energy, 2015, 13, 670–678.
27 Z. Stevi´c, M. Raj˘ci´c-Vujasinovi´ J. Power Sourc., 2006, 160 1511–1517.
28 H. M. Pathan and C. D. Lokhande, Bull. Mater. Sci., 2004, 27(2), 85-111.
29 S. D. Sartale and C. D. Lokhande, Mat. Chem. Phy., 2000, 65, 63–67.
30 Comprehensive Coordination Chemistry, Wilkinson, G. Ed.; Pergamon Press: Oxford, U.K., 1987, 5, 71.
31 Y. Wu, C. Wadia, W. Ma, B. Sadtler and A. Alivisatos, Nano Lett., 2008, 8, 2551-2555.
32 D. P. Dubal, G. S. Gund, R. Holze, and C. D. Lokhande J. Power Sour. 2013, 242,687-698.
33 Handbook of X-ray photoelectron spectroscopy, C. D. Wagner, W. M. Riggs, L. E. Davis, J. F. Moulder, J. E. Muilenberg, Perkin-Elmer Corporation U.S.A. 1979.
34 C. Plackowski, M. A. Hampton, W. J. Bruckard and A. V. Nguyen, Miner. Eng. 2014, 55, 60–74.
35 Y. Su, X. Lu, M. Xie, H. Geng, H. Wei, Z. Yang and Y. Zhang, Nanoscale, 2013, 5, 8889-8893.
36 H. Tang, Y. He, B. Li, J. Jung, C. Zhang, X. Liu and Z. Lin, Nanoscale, 2015,7, 9731-9737.
37 J. Liu, X. Huang, Y. Li, K. M. Sulieman, X. Heb and F. Sun, J. Mater. Chem., 2006, 16, 4427–4434.
38 H. D. Tran J. M. D'Arcy, Y. Wang, P. J. Beltramo, V. A. Strong and R. B. Kaner, J. Mater. Chem., 2011, 21, 3534–3550.
39 Y. K. Hsu, Y. C. Chen and Y. G. Lin, Electrochimica Acta, 2014, 139, 401–407.
40 D. P. Dubal, G. S. Gund, C. D. Lokhande and R. Holze, ACS Appl. Mater. Inter., 2013, 5, 2446−2454.
41 S. J. Patil, V. S. Kumbhar, B. H. Patil, R. N. Bulakhe and C. D. Lokhande, J. Alloy. Compd., 2014, 611, 191–196.
42 K. J. Huang, J. Z. Zhang and Y. Fan, J. Alloy. Compd., 2015, 625, 158–163.
43 C. Shi, Q. Zhao, H. Li, Z. Liao and D. Yu, Nano Energy, 2014, 6, 82–91.
44 P. Velasquez, D. Leinen, J. Pascual. J. R. R. Barrado, P. Grez, H. Gomez, R. Schrebler, R. D. Rıo and R. Cordova, J. Phys. Chem. B, 2005, 109,4977-4988.
45 M. Jayalakshmi, M. M. Rao and B. M. Choudary, Electrochem. Comm., 2004, 6, 1119–1122.
46 F. Tao, Y. Q. Zhao, G. Q. Zhang and H. L. Li, Electrochem. Comm. 2007, 9, 1282–1287.
47 Z. Yang, C. Y. Chen and H. T. Chang, J. Power Sourc., 2011, 196, 7874–7877.
48 A. M. Wang, H. L. Wang, S. Y. Zhang, C. J. Mao, J. M. Song, H. L. Niu, B. K. Jin and Y. P. Tian, Appl. Surf. Sci., 2013, 282, 704-708.
49 X. Li, J. Shen, N. Li and M. Ye, J. Power Sourc. 2015, 282, 194-201.

RSC Advances Accepted Manuscript

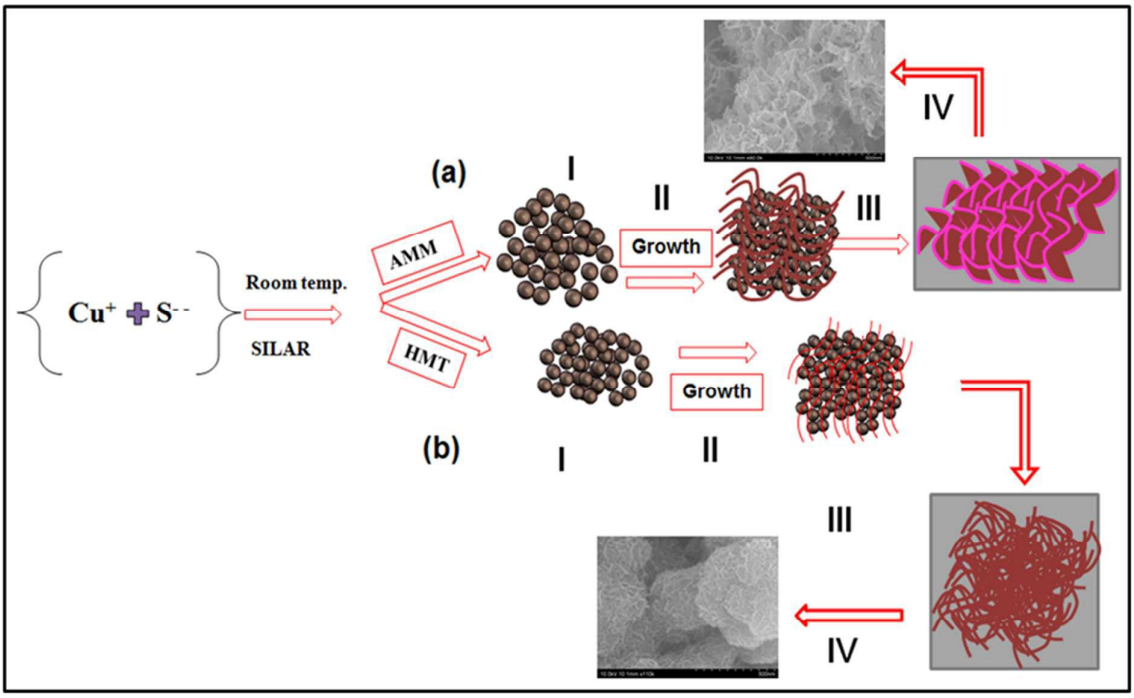


Fig. Schematic growth of copper sulfide as nanoflakes and nanotube like structure.

RSC Advances Accepted Manuscript